A&A 454, 517–526 (2006)
DOI: 10.1051/0004-6361:20064881

Astronomy & Astrophysics

10^{51} erg less: the Galactic H II region OA 184

T. Foster[1], R. Kothes[1,2], X. H. Sun[3], W. Reich[4], and J. L. Han[3]

[1] National Research Council of Canada, Herzberg Institute of Astrophysics, Dominion Radio Astrophysical Observatory, PO Box 248, Penticton, BC, V2A 6J9, Canada
e-mail: Tyler.Foster@nrc-cnrc.gc.ca
[2] Department of Physics and Astronomy, University of Calgary, 2500 University Drive N.W., Calgary, AB, Canada
[3] National Astronomical Observatories, Chinese Academy of Sciences, Beijing 100012, China
[4] Max-Planck-Institut für Radioastronomie, Auf dem Hügel 69, 53121 Bonn, Germany

Received 19 January 2006 / Accepted 13 March 2006

ABSTRACT

Aims. The identification of the object OA 184 as a Galactic Supernova Remnant (SNR) is re-examined, and evidence to the contrary is presented. The aim is to show definitively that OA 184 is actually a Galactic H II region, and to estimate some physical parameters for the nebula (e.g. temperature, density, and magnetic field in the ionized shell).
Methods. To determine the broad spectral properties of OA 184 a multiwavelength approach is used, with historical and new radio data, and existing X-ray and IR data on OA 184 considered. Radio continuum 408 and 1420 MHz Canadian Galactic Plane Survey (CGPS) data, Effelsberg 2695 MHz data, and new Urumqi 5 GHz radio observations in Stokes I, Q, and U are presented. As well, we present CGPS H I line data, and eight radio recombination lines (RRL, H103-110α) observed for this study with the Green Bank Telescope.
Results. An integrated radio spectrum of index $\alpha = -0.14$ to -0.2 ($S(\mathrm{Jy}) \propto \nu^{\alpha}$) is determined from four radio frequencies. RRL emission appears at $v_{\mathrm{LSR}} = -25.8$ km s^{-1} and at the intensity predicted for free-free thermal emission. Q and U maps at λ 6 cm show OA 184 as a depolarizing source, affecting a background filament of polarized non-thermal Galactic emission. An H II shell of thickness less than 0.2° is indicated by this depolarization. CGPS ~1-arcminute resolution H I line maps are presented, and the systemic velocity of the ISM immediately surrounding OA 184 is -26.8 km s^{-1}. The distance of OA 184 is 2.2 ± 0.4 kpc, obtained from a new distance method based on a Galactic H I modelling procedure. A simple model as a shell of ionized hydrogen 4 pc thick is considered, and the RRL observations are used to estimate (under conditions of non-thermodynamic equilibrium) the electron temperature $T_{\mathrm{e}} = 8300$ K and density $n_{\mathrm{e}} = 5.3$ cm^{-3}. The line of sight magnetic field in the ionized shell is found to be $\langle B_{\parallel} \rangle \simeq -2.5\,\mu$G (directed away from the Sun).
Conclusions. We conclude that OA 184 is a Galactic H II region energized by the lone O7.5V star BD+41°1144.

Key words. polarization – ISM: supernova remnants – H II regions

1. Introduction

Supernova remnants mark the impact of the most dynamic processes on ISM material. By a very simple calculation, Padmanabhan (2001) found at least half of the Galactic ISM has been occupied at one time by a SNR, so pointing a telescope virtually anywhere in the plane shows a beam filled with SNR-processed matter. Since it is suspected that in current radio surveys only a fraction of SNR are actually detected, accounting for *every* SNR in any given region of the disk is *paramount* to a proper description of the ISM. In particular, the energy input into the anticentre region of the Galactic disk will be dominated by remnants in the Perseus Spiral arm, so even one less such object here dramatically affects the local energy budget.

In the Galactic plane near the anti-centre region $\ell = 165°$, $b = +3°$ three conspicuous objects reside within about 5 degrees of one another; HB 9 (G160.9+2.6), VRO 42.05.01 (G166.0+4.3) and OA 184 (G166.2+2.5). These are all classified as supernova remnants in Green's Catalogue of Galactic SNRs (Green 2004). In particular, OA 184 (the optical portion is referred to as Sh2-223 in Sharpless 1959) has a large apparent diameter ($90' \times 70'$), and due to an apparently great distance (8 kpc suggested by Routledge et al. 1986) is thought to be one of the largest SNRs in the sky (200 pc diameter). It was first identified as a possible SNR by Dickel & Yang (1965).

From the collection of literature on the object, it would seem that OA 184 has very strange and extreme properties as a Galactic SNR, especially when compared to its neighbors VRO 42.05.01 and HB 9. Besides being quite distant into the anticentre, it exhibits no X-ray emission (see Fig. 1), is not at all seen in low frequency radio surveys (such as the 151 MHz Cambridge survey, Vessey & Green 1998; and Fig. 1), is *distinctly* visible in infrared surveys as a dusty shell that traces the radio shell (Fig. 5, IGA IRAS data part of the CGPS, Taylor et al. 2003), and has an optical spectrum with line ratios uncharacteristic of SNRs (Fesen et al. 1985). However, no one seems to have questioned its identity as a supernova remnant. While SNR evolutionary models certainly can be applied to it (and return physical parameters within reason for any SNR, e.g. Routledge et al. 1986; Leahy & Marshall 1988), this is not sufficient for the SNR classification.

In this paper we present a multiwavelength body of evidence that OA 184 is an H II region, and has been misclassified as an SNR. This evidence comes from re-examination of available data and literature, and by two new radio observations of OA 184 near 5 GHz: 1) polarized continuum emission; and 2) radio recombination line (or RRL). These observations are chosen to

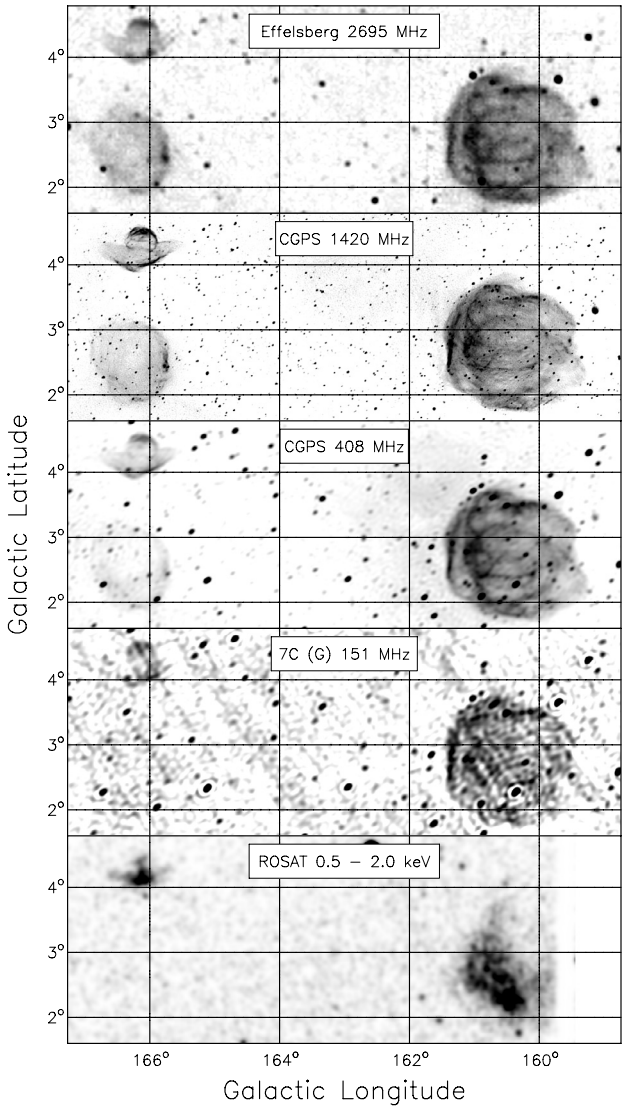

Fig. 1. A multi-wavelength view of OA 184 (G166.2+2.5), VRO 42.05.01 (G166.0+4.3) and HB 9 (G160.9+2.6), at (*top to bottom*) 2695 MHz, 1420 MHz, 408 MHz, 151 MHz, and X-ray (ROSAT All-Sky Survey). This figure demonstrates the unexpectedly different emission characteristics of OA 184 from the two known SNRs VRO 42.05.01 and HB 9.

be particularly telling in the following sense; 1) polarized emission at 6 cm *should* be observed even for a remnant that is well into the radiative evolutionary phase; and 2) recombination lines from a SNR shock *should* be very much weaker than the level produced by a cooler and completely thermal plasma. Among other things, the RRL observations allow a new direct velocity measurement for the object, and the depolarizing nature of the object allows an estimate for the line-of-sight magnetic field in the ionized shell to be made, the first such measurement in an H II region made using the Galactic background itself as the polarized source.

2. A brief analysis of historical data on OA 184

OA 184 has been described as a Galactic SNR, first by Dickel & Yang (1965). This classification is furthered on the basis of an apparently steep radio spectrum (Haslam & Salter 1971, find $\alpha = -0.55 \pm 0.15$). Routledge et al. (1986) conclude the same

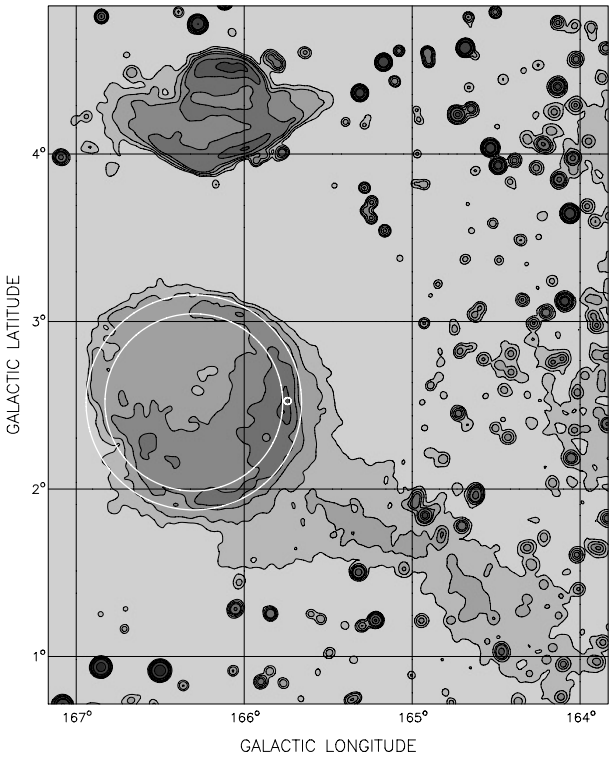

Fig. 2. A 3′ resolution λ21 cm view of the Galactic plane near OA 184 (G166.2+2.5) and VRO 42.05.01 (G166.0+4.3). Point sources around OA 184 have been removed (see Sect. 5.2). A circle of radius $\theta = 0.64°$ well delineates the shell, whose thickness is approximately defined between that and an inner circle of radius $\theta_{\rm inner} = 0.53°$. The centre and beamwidth of the GBT search for RRL emission is shown as the small circle through the shell's West wall.

non-thermal nature for the emission ($\alpha = -0.54 \pm 0.1$). These two studies are anchored by a low-frequency point in their calculations; the integrated flux from the 38 MHz survey of Williams et al. (1966). The radio object has received recent attention by Leahy & Tian (2005), who from 21 cm and 74 cm Canadian Galactic Plane Survey (CGPS) data, determine that OA 184 partially sits atop a "tongue" of non-thermal emission extending in from the SW. After correcting for this background and eliminating flux contributed by compact sources within the object's boundary, they determine $\alpha = -0.32 \pm 0.06$ (38 MHz to 2700 MHz), and -0.25 ± 0.03 (408–1420 MHz only).

The object is a distinct, nearly circular shell in 21 cm and 74 cm radio continuum data (see Fig. 2 for 21 cm appearance), though its emission is modest (on average 0.5 and 5 K above background respectively). Circles of radius 0.64° and 0.53° are fitted by eye to the 21 cm map and are shown in Fig. 2.

A multiwavelength look at OA 184 and surroundings is shown in Fig. 1. The nearby SNRs VRO 42.05.01 and HB 9 are clearly strong sources at all frequencies, whereas OA 184 fades to invisibility in the low frequency 151 MHz survey (by integrating the background in these data we determine an upper-limit to the 151 MHz flux density, Sect. 5.2). Low-frequency radio emission from the shell is *not* observed at 38 MHz (in the maps of Williams et al. 1966). Rather, the synchrotron tongue introduced by Leahy & Tian (2005) is the only source of emission at the location of OA 184; however this extends many degrees beyond OA 184's bounds, and is clearly unrelated. VRO 42.05.01 and HB 9 are very distinct and bright sources in the 38 MHz maps, despite the low resolution of this survey (≃45′). One must then question what Haslam & Salter (1971) were actually measuring.

Inspection of the maps of Williams et al. (1966) suggests that the 38 MHz flux point obtained by Haslam & Salter (1971) must in fact be only that of the synchrotron tongue's tip at OA 184's location. The inclusion of the 38 MHz flux point in OA 184's radio spectrum is therefore questionable. The radio spectrum of OA 184 is found to be flatter after discarding the 38 MHz flux density.

The shell-nature of the radio emission is also very apparent in IRAS 60 and 100 μm images taken from the CGPS database (Taylor et al. 2003), on average 2 and 7 MJy per steradian above background ($\sigma_{\rm bg} \sim 0.2$ and 1.1 MJy rad^{-2} in these respective bands). There is no IRAS emission apparent in either band from nearby remnants VRO 42.05.01 and HB 9. Through Sedov evolutionary models applied to these IR data, Leahy & Marshall (1988) conclude that OA 184 is an old remnant, well past the adiabatic phase of SNR expansion (Woltjer 1972) and into radiative cooling.

A very advanced age would seem to make sense from this predominant IR and lack of X-ray emission observed for OA 184 (see Figs. 5 and 1 respectively), as it suggests that nearly all of the kinetic energy in the shock has been thermalized. The broken shell-like structure characteristic of the IR appearance is also visible in optical (DSS) red plates, unmistakably tracing Hα emission from OA 184 (e.g. see Fich et al. 1990). While not unusual for a radiative SNR, Fesen et al. (1985) note that the Hα emission dominates other lines (e.g. [S II], [O III]), commenting that the optical spectrum is more reminiscent of an H II region. Binette et al. (1982) even suggest that H II region emission contaminates the spectrum of OA 184. The optical emission from this object could support the old-SNR idea of Leahy & Marshall (1988), as only a radiative shock model can produce the observed optical line intensities with an elemental abundance less than that of the SNRs in the LMC (Binette et al. 1982).

However, even radiative-phase SNRs still exhibit characteristic X-ray emission and radio polarization. No X-ray emission on OA 184 is observed in the ROSAT All-Sky Survey down to the background fluctuations (see Fig. 1), whereas VRO 42.05.01 and HB 9 are strong X-ray sources. As well, no polarization for OA 184 is observed in CGPS 21 cm Q and U maps, whereas both HB 9 and VRO 42.05.01 are distinct sources of linearly polarized emission. It is significant to note that these three sources are all Perseus arm objects, and therefore at similar distances. One would expect the same absorption column in the foreground to affect these SNRs, and similar Faraday screens to scramble any well-ordered polarized radio emission from them. Why then are HB 9 and VRO 42.05.01 so vastly different from OA 184?

While all this evidence strongly hints at a misclassification for OA 184, in itself it may not be sufficient to overturn the old SNR idea. We now turn to a new body of observational evidence for answers.

3. Observations and data reduction

3.1. CGPS radio continuum observations

New observations of OA 184 at 408 and 1420 MHz are made as part of the Canadian Galactic Plane Survey (Taylor et al. 2003). The Synthesis Telescope (ST) at the Dominion Radio Astrophysical Observatory (DRAO) is the principal instrument for these observations. The FWHM of the synthesized beam are $49'' \times 49''$ cosec δ and $2.8' \times 2.8'$ cosec δ resolution at 1420 MHz and 408 MHz, respectively. Continuum data at 21 cm have an intrinsic uncertainty due to calibration of ±5%, and are ±10% uncertain at 74 cm. Other relevant parameters of the DRAO ST can be found in the paper by Landecker et al. (2000). 21 cm continuum data are shown in Fig. 2 while the 74 are presented in the recent publication by Leahy & Tian (2005). In this paper we also review the 21 cm neutral hydrogen line observations (see Fig. 4).

In addition to CGPS total power observations, we present new observations of OA 184 in Stokes I, Q, U and several α-recombination lines at 6 cm wavelength. These are described below in more detail.

3.2. 6 cm Stokes I, Q, U observations

The mapping observations of OA 184 at $\lambda = 6$ cm were conducted in January, March, and September, 2005 with the 25 m telescope of the Urumqi Astronomical Observatory, which is part of the Chinese Academy of Science. The telescope is equipped with a receiving system constructed by the Max-Planck-Institut für Radioastronomie, which is intended for a survey of the polarization of the Galactic plane at 6 cm, providing maps at all Stokes parameters with an angular resolution of 9.5′. The central frequency is 4.8 GHz with a bandwidth of 600 MHz. All maps were scanned along Galactic longitude or latitude with a size of $2^\circ \times 2^\circ$ centered at $(\ell,\ b) = (166.3, +2.5)$. As the primary calibrator we used 3C 286 with a flux density of 7.5 Jy, a polarization angle of 33°, and a polarization percentage of 11.3%.

The data reduction procedure is described in Sun et al. (2006). In brief, the baselines are corrected by setting the ends of each subscan to zero, spikes of interference are edited out, and scanning effects are suppressed by unsharp masking. Then all individual coverages observed in the two scanning directions are combined together in the Fourier domain (see Emerson & Gräve 1988).

3.3. Radio recombination line observations and reduction

Radio recombination line (RRL) observations towards the brightest continuum filament on OA 184 were obtained on 6 and 20 Dec. 2005 with the 100 m Green Bank Telescope. The pointing is shown in Fig. 2. As a check of the system's ability to record RRL emission, the bright H II source Sh2-206 was observed for 5 min at the beginning of each observation. This source has the following known line characteristics at 3 cm: $T_{\rm line} = 68$ mk, $v_{\rm LSR} = -25.2$ km s^{-1} and $\Delta v = 26.6$ km s^{-1} (Lockman 1989). At 5.4 GHz (H106α) the predicted line temperature of Sh2-206 is approximately 244 mK.

The objective was to search for α-line radio recombination emission from hydrogen at C-band (4–6 GHz). A signal at the level predicted from assuming thermal emission would confirm the object as thermal. SNRs can also have observed RRL emission (from the cooling filaments behind the shock, for example), but the line-to-continuum ratio is observed to be much smaller for SNRs (e.g. 0.001, SNR W 49 B, Downes & Wilson 1974). We predict the line intensity of RRL emission from OA 184 as follows. First, the 1420 MHz continuum map is convolved to the resolution of the GBT (2.5′ at 5.4 GHz). The brightest continuum filament belonging to OA 184 (see white circle, Fig. 2) appears 1 K above background at 21 cm. By assuming thermal emission ($\alpha = -0.1$), we extrapolate this brightness to 60 mK at 5.4 GHz. A line temperature of 2.2 and 1.8 mK (at 4.8 and 5.9 GHz respectively) is found from the line-to-continuum ratio for thermal emission (~0.035, see Eq. (12.24) Rohlfs 1986),

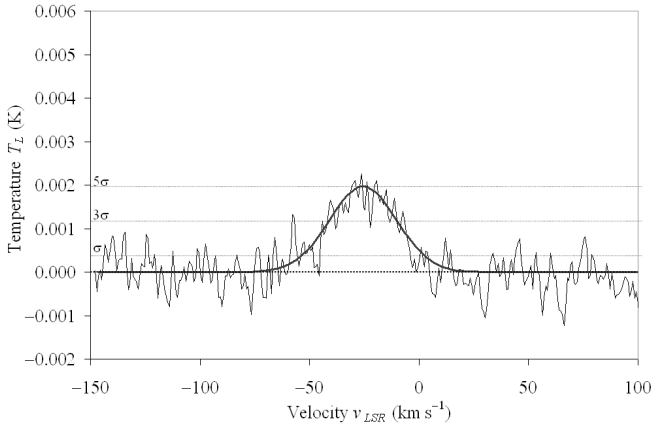

Fig. 3. Radio recombination line emission from OA 184. This is a composite spectrum of seven transitions in hydrogen (H103, 105-110α). The peak line temperature is 2 mK, 5σ above the rms noise (lines for which at 1, 3 and 5σ are shown).

assuming $T_e = 10^4$ K and a more-or-less normal linewidth of 30 km s^{-1} (e.g. see Lockman 1989). A 50 MHz bandwidth receiver is used to allow eight recombination lines to be simultaneously observed (H103-110α) in the high end of the *C*-band (ν = 4.8–5.9 GHz). Both polarizations were admitted, and the spectrum consists of 4096 channels (0.62–0.75 km s^{-1} per channel). For both observations (frequency switched, 8100 s total integration on-source) the expected rms noise is $\Delta T_{\rm rms} \sim 1.5$ mK, as the system temperature in this band is typically ∼20 K for elevations of 30° or higher.

Seven of the eight bands were not affected by RFI (the exception was H104α at 5.76 GHz; this band was not usable). RRL emission from the source Sh2-206 is strongly visible in each band, and has fitted line properties similar to those at 3 cm (Lockman 1989): for example for H106α $T_l = 261 \pm 2$ mK, $v_{\rm LSR} = -25.7 \pm 1$ km s^{-1}, and $\Delta v = 27.9 \pm 2$ km s^{-1}. After averaging both linear polarizations together a cubic baseline was fitted and removed from each observation. Each of the spectra were then regridded in velocity space to a common channel width (0.75 km s^{-1}). To increase the sensitivity, these regridded spectra are combined into one composite velocity spectrum. The combined detection is at a level $T_{\rm line}/\Delta T_{\rm rms} = 5$ ($\Delta T_{\rm rms} = 0.4$ mK, $T_{\rm line} = 2.0 \pm 0.2$ mK). Here $\Delta T_{\rm rms}$ is the rms deviation of the baseline portion of the spectra. The signal from OA 184 occurs at a velocity of $v_{\rm LSR} = -25.8 \pm 0.6$ km s^{-1} and has a full width (to half intensity points) of $\Delta v_{\rm line} = 34.7 \pm 4.6$ km s^{-1}. The uncertainties in these values were estimated from 100 synthetic noisy spectra, simulated using a Monte-Carlo approach with a normal distribution of width $\sigma_{\rm rms} = 0.4$ mK. Gaussians were fitted to them, and the variance in each fitted parameter defines the above uncertainties. The composite spectrum and fitted Gaussian are shown in Fig. 3.

4. Neutral hydrogen and a new distance to OA 184

The interstellar medium in neutral hydrogen around OA 184 was imaged in detail (resolution $1' \times 1.4'$) by Routledge et al. (1986). The observing instrument was the previous 4-element incarnation of the DRAO interferometer. The area has been re-imaged for the CGPS by the modern 7-element DRAO ST, with a higher velocity resolution (1.3 km s^{-1}) and greater brightness temperature sensitivity ($\Delta T_{\rm b} = 3$ K). These new observations are presented in Fig. 4; each $T_{\rm b}(\ell,\ b)$ slice is the average of 2 channels in velocity. The H I filaments on OA 184's North-Western face reported by Routledge et al. (1986) (cf. Fig. 4 in that paper) are much more apparent in the CGPS data. In the new maps a 90° segment of a circular shell curves with the radio continuum contours from twelve o'clock to 3 o'clock can be seen in channels −25.2 and −26.8, whereas at −28.4 km s^{-1} this feature extends from one o'clock to three o'clock. We believe that −26.8 km s^{-1} is the best *systemic* velocity that can be estimated from the new maps, as here the shell's expansion velocity (if any) will be directed perpendicular to the line of sight.

A kinematic distance of 8.7 kpc is found from this velocity estimate and a flat rotation curve with $R_0 = 7.9$ kpc (Eisenhauer et al. 2003), and $v_0 = 220$ km s^{-1}. However, this assumes that the systemic $v_{\rm LSR}$ is the observed component of circular rotational motion only. In the Galactic anticentre, the line of sight is not overly sensitive to such motions; rather, it is overwhelmingly sensitive to *radial* motions (those directed towards the Galactic centre). A kinematic-based distance method that accounts for both circular and radial motions has been developed by Foster & MacWilliams (2006). Their approach has the advantage of being based on a model Galactic H I distribution and rotation curve that has been fitted to observations, rather than on an assumed purely circular model (see Foster & MacWilliams 2006, for details on the application of their H I modelling method). A distance of 2.2 ± 0.4 kpc results from this method. This is in agreement with the estimate of ∼2 kpc (Fesen et al. 1985) based on the extinction to the optical filaments (Sh2-223), and the very recent astrometric distance to W3OH (a known Perseus arm maser near $\ell = 130°$) of 1.95 ± 0.04 kpc by Xu et al. (2006).

Koo & Heiles (1991) performed a study of H I emission towards 103 sources believed to be supernova remnants in order to find rapidly expanding SNR shells. They detected high velocity H I for 15 objects in their sample, among those OA 184. If OA 184 is an H II region a connection with this high velocity gas ($v < -130$ km s^{-1}) is not feasible, since any embedded star(s) could not be expected to accelerate gas to such a high velocity. To investigate the origin of this high velocity gas we examined data from the Leiden-Dwingeloo H I survey (Hartmann & Burton 1997). We find a high velocity cloud (HVC) complex that stretches from $150° \le \ell \le 180°$, $0° \le b \le +1°$ and covers a velocity range -150 km s$^{-1} \le v \le -110$ km s^{-1}. The high velocity H I cloud detected towards OA 184 by Koo & Heiles (1991) is more likely to be a member of this HVC complex than just an isolated patch of SNR-accelerated H I.

5. The 4.8 GHz radio continuum observations of OA 184

Here we present an analysis of the new λ 6 cm continuum and polarization observations. The new 6 cm flux density of OA 184 is considered along with other historical data in determining the radio spectrum of the object. A lack of linearly polarized emission from OA 184 itself is discussed, along with its apparent affect on the distinctly polarized synchrotron filament superposed on the face of OA 184.

5.1. The λ 6 cm appearance of OA 184

In Figs. 5 and 6 we display radio continuum images of OA 184 in total power and polarized intensity, observed with the Urumqi 25 m telescope at 4.8 GHz. The structure of the total power emission resembles that of an almost circular shell quite typical for a shell-type supernova remnant. However, even at a frequency

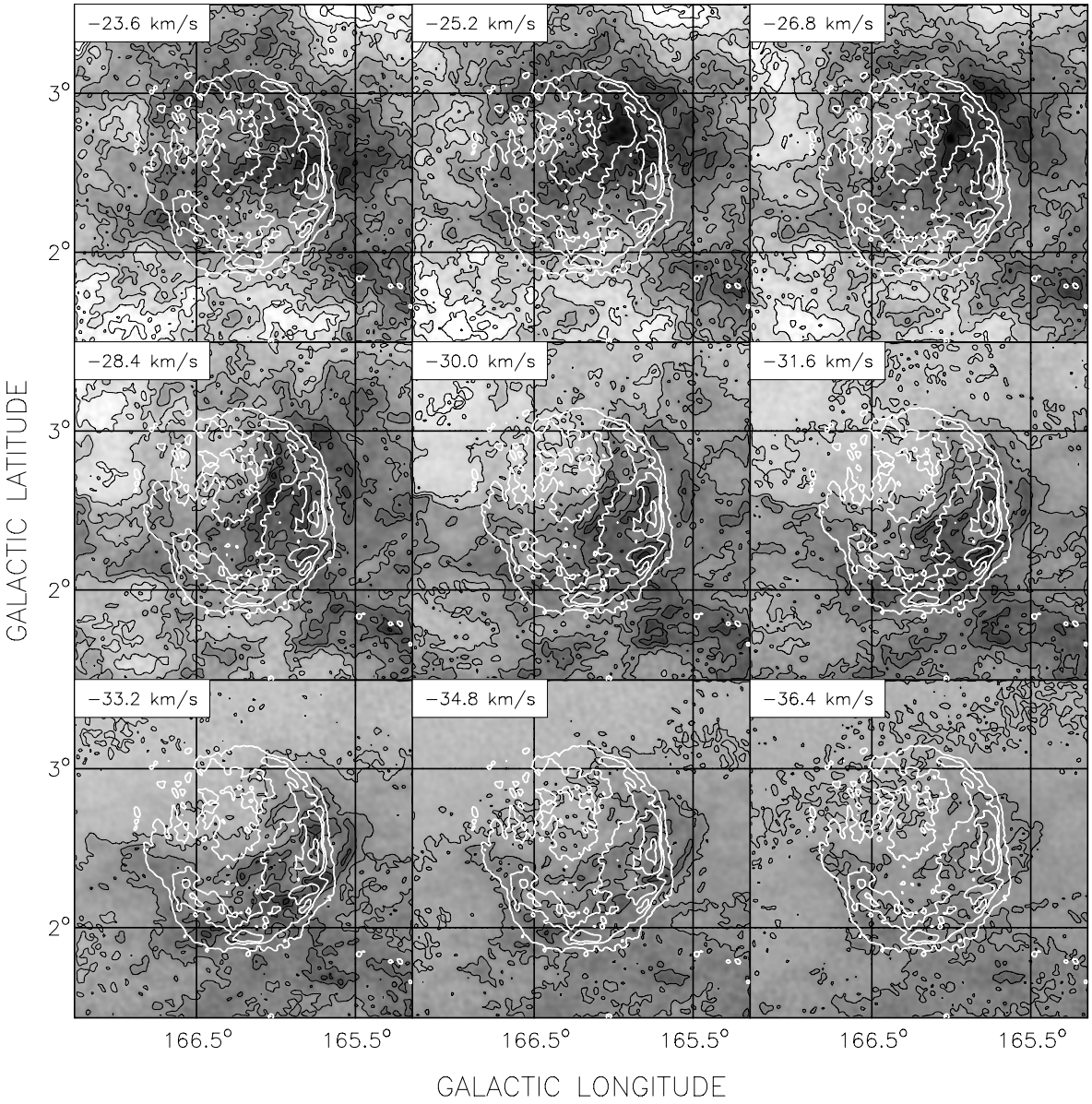

Fig. 4. Montage of nine H I channel maps from the CGPS towards OA 184. The systemic velocity of the ISM surrounding OA 184 was estimated by Routledge et al. (1986) at -30 km s^{-1}; RRL observations of the ionized gas (this paper) show -26 km s^{-1} (see Fig. 3).

as high as 4.8 GHz the emission seems to be unpolarized. If we compare the peak of the total power emission of 52 mK with the contour levels displayed in the polarized intensity image we derive a maximum percentage polarization of 1.5% for a 4σ signal. On the other hand the two other nearby supernova remnants VRO 42.05.01 and HB 9 are highly polarized in the data of the CGPS at a frequency of 1420 MHz, with overall percentage polarizations of 8.6 and 9.1% respectively (Kothes et al. 2006). At this frequency the rotation of the polarization angle would be 11 times higher than at 4.8 GHz for the same rotation measure (RM). All of these three objects are believed to be in the Perseus arm at about the same distance from us.

If we take a closer look at the structure of the observed polarized emission we actually see that it is brightest where the total power emission is faintest, outside and in the centre of OA 184. The little structure at $\ell = 166\overset{\circ}{.}7$ and $b = 2\overset{\circ}{.}3$ is an extragalactic background source. This inverse relation between total power and polarized intensity is more indicative of a depolarization rather than an emission feature. In the 1420 MHz total power image in Fig. 2 it looks like the synchrotron filament enters OA 184 in the lower right quarter. The positional coincidence of this filament with the polarized patch outside OA 184 (see Fig. 6) indicates that this filament is the actual source of the polarized emission. The gap between the two polarization patches is created by depolarization through the shell of OA 184 where the path length is longest. This also indicates that the synchrotron filament is located behind OA 184.

In the following we will discuss the radio spectrum of OA 184 and the possibility of it being an object that depolarizes synchrotron emission coming from behind it.

5.2. The radio spectrum of OA 184

Because of the significant contribution of the synchrotron filament in the Galactic plane in the direction of OA 184, the flux densities found by many observers may be biased

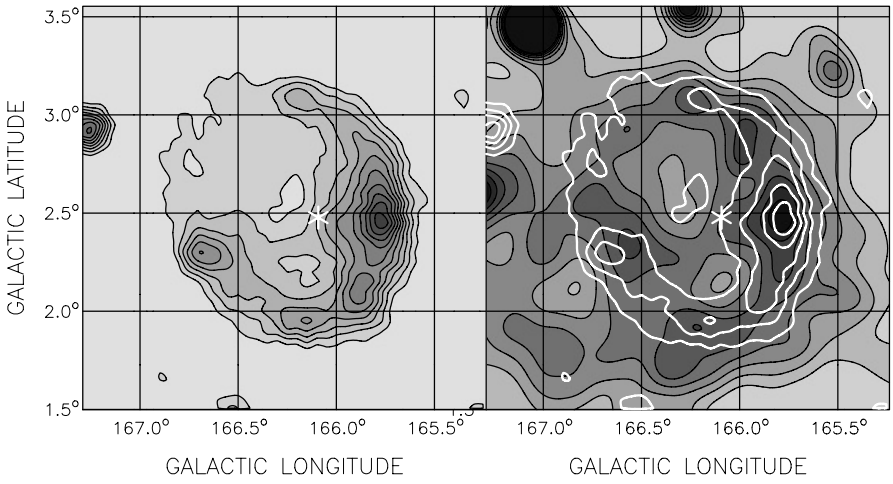

Fig. 5. Total power radio continuum image of OA 184 observed with the Urumqi 25 m telescope at a frequency of 4.8 GHz (*left*) and 60 μm image from the IRAS survey taken from the CGPS database (*right*). Radio contours (in black, *left*) are shown from 5 to 50 mK in steps of 5 mK, and IR contours at 2.0, 2.3, 2.6, 2.9, 3.2, 3.5, 3.8, and 4.1 MJy/sr are shown at right (black), and are overlaid with white radio contours from 5 to 45 mK (in steps of 10 mK). The position of the O7.5V star BD+41°1144 is indicated by the white asterisk.

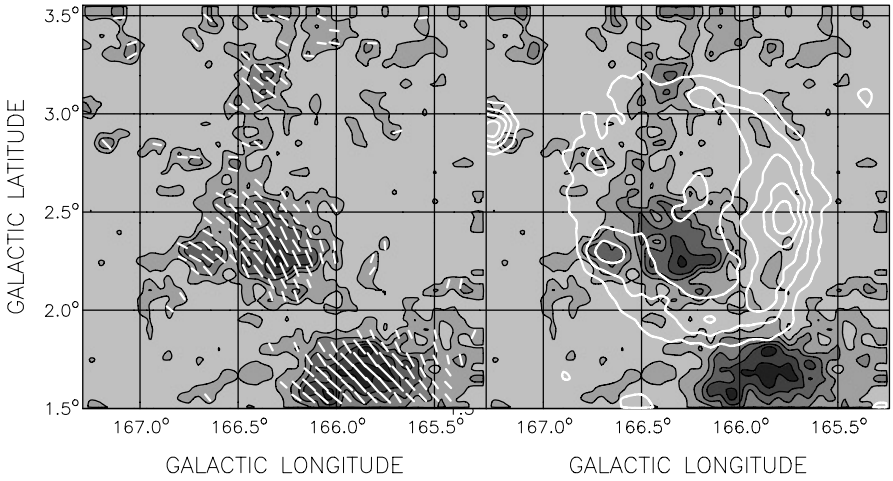

Fig. 6. Linearly polarized intensity image of OA 184 observed with the Urumqi 25 m telescope at a frequency of 4.8 GHz. Contour levels are at 4, 6, 8, 10, 12, and 14σ (σ = 0.2 mK). *Left*: overlaid vectors are E-field direction with a length proportional to polarized intensity. *Right*: white contours indicate total power emission.

(e.g. Haslam & Salter 1971). Therefore, to obtain an accurate spectrum we have analyzed only measurements for which the original data were available to us to allow consistent treatment of the zero levels.

As already mentioned by Leahy & Tian (2005) there are two main problems which make the determination of a reliable flux density of OA 184 quite challenging. These are the contribution of numerous extragalactic point sources that are projected onto OA 184 and a tongue-like filament of diffuse synchrotron emission that overlaps OA 184. Both problems if not taken care of could steepen the spectrum of the source significantly and make a proper flux density integration from a low resolution observation virtually impossible. To determine a reliable radio spectrum we used all available data at sufficient resolution, which are our 4.8 GHz measurement, the 1420 MHz and 408 MHz data from the Canadian Galactic Plane Survey, and the 2.7 GHz data from the Effelsberg survey (Fürst et al. 1990). We also obtain an upper limit flux density from 151 MHz data (Vessey & Green 1998).

We removed the point sources from the CGPS measurements and the 2695 MHz Effelsberg survey by fitting Gaussians to them. In the 4.8 GHz data with a resolution of 9.5′ the point sources are not visible, distinct from OA 184's emission due to the lower resolution and the lower flux density. Most of these have rather steep spectra. We used the flux densities published by Leahy & Tian (2005), extrapolated their flux densities to 4.8 GHz and subtracted these from our integrated values.

To integrate the flux density of OA 184 we determined radial profiles of the radio emission starting at its centre of $\ell = 166\overset{\circ}{.}3$ and $b = +2\overset{\circ}{.}53$. We produced 4 profiles at each frequency, covering each quarter of the source individually (see Fig. 7, left, for 1420 MHz profiles). These quarters are separated by the angles 0, 90, 180, and 270° west of north. This was done to remove background emission more reliably. Especially the lower right quarter of the source seems to be strongly contaminated by the synchrotron filament as indicated by the presence of the bright polarized patch in the 4.8 GHz observations (see Fig. 6). However, the upper right and the lower left quarter showed some enhanced background as well especially at 408 MHz where the synchrotron filament should be brightest. After removal of the background emission, which was done individually in each

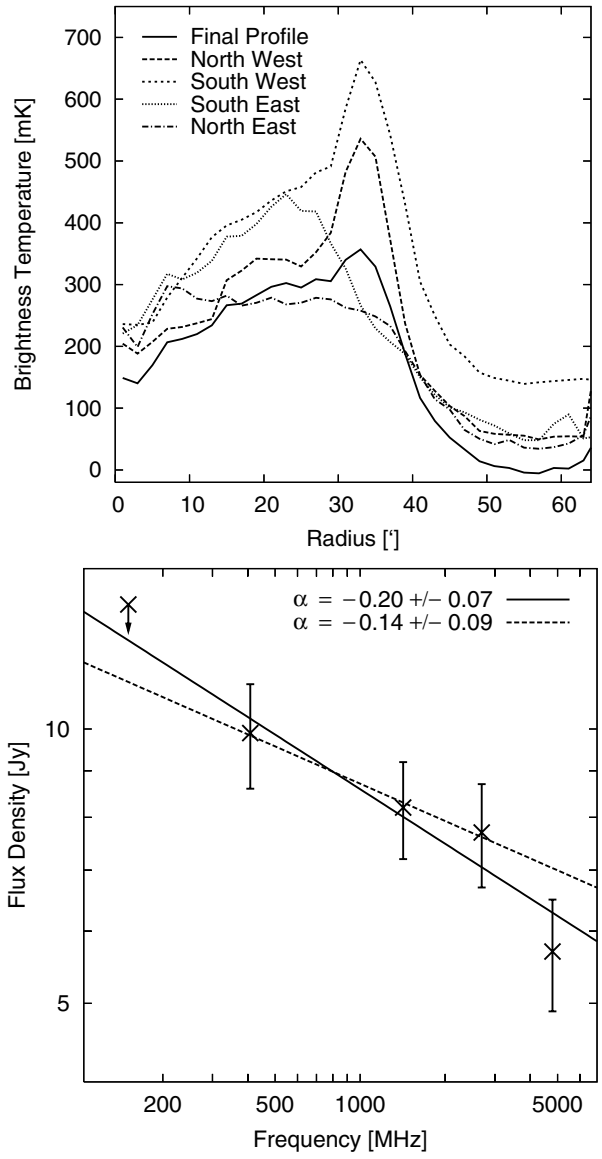

Fig. 7. *Top*: radial brightness temperature profiles at 1420 MHz. Shown are the four raw profiles for each individual quadrant and the final profile after background subtraction and averaging. The radial profiles were calculated in steps of 2 arcmin. *Bottom*: integrated radio spectrum of OA 184 calculated between the 4 frequencies used here. An upper-limit flux density at 151 MHz is also shown, estimated by integrating successively larger rings centred on OA 184 in the data (see Fig. 1) out to where only background is present. This data point is not used in the fit, as it is only an upper-limit for an object that is buried by background fluctuations. The solid line represents a fit to data at four frequencies (408–4850 MHz) and the dashed line between the three lower frequencies only.

quarter by averaging the rings outside the emission attributed to OA 184, the four profiles for each frequency were averaged. Integrated flux densities under those profiles are given in Table 1, and the resulting radio spectrum is shown in Fig. 7 (right panel).

Additionally we used the data from the 7C(G) survey of the Galactic Plane at 151 MHz (Vessey & Green 1998) (see Fig. 1). In this image OA 184 is not visible. However, we fitted Gaussians to all point sources visible in the area where OA 184 should be and removed them. Then we integrated the flux in the area of OA 184 by calculating a radial profile starting from the centre at $\ell = 166.^{\circ}3$ and $b = +2.^{\circ}53$ (see above). We determined a

Table 1. The integrated flux density of OA 184 at four radio frequencies. All values are calculated for this paper from original data. Fluxes of small diameter sources and the synchrotron ridge that the object sits atop (Leahy & Tian 2005) were removed prior to the integration of the continuum brightness temperature. The 151 MHz flux density is an upper limit (see text).

ν (MHz)	S (Jy)
151	13.7 ± 3.0
408	9.9 ± 1.3
1420	8.2 ± 1.0
2695	7.7 ± 1.0
4800	5.7 ± 0.8

constant background as described before for the individual quarters. This flux density should be an upper limit since only very few point sources are visible and more important the synchrotron filament was not removed. The resulting flux density is listed in Table 1 and we added this data point to Fig. 7. This upper limit supports the flat spectrum determined with the four higher frequencies.

Although the overall shape of the 4.8 GHz profile is very similar to the others, the flux density seems to be consistently less. This can also be seen in the radio spectrum. The likely reason for this is that the 2° maps we observed at this frequency were too small. In the 4.8 GHz observations we remove a baseline by arbitrarily setting the ends of each subscan to 0. This means that structures bigger than about 90–100′ may be missing. As a result the radial profile and the flux density at this frequency would be below the others. The spectral index fitted between all four frequencies results in −0.20, and without the 4.8 GHz value −0.14 (see Fig. 7). The errors for the flux densities accounts for the uncertainty in the background determination and that of the flux calibration. Our flux densities (see Table 1) agree very well with those derived by Leahy & Tian (2005). This spectral index favours a thermal origin for the radio emission of OA 184.

We also calculated TT-Plots between the radial profiles to confirm the thermal spectrum. The result is $\alpha = -0.13 \pm 0.06$ with a maximum of $\alpha = +0.1 \pm 0.2$ between 1420 MHz and 2695 MHz, and a minimum of $\alpha = -0.3 \pm 0.2$ between 1420 MHz and 4.8 GHz. This additionally points to the thermal nature of OA 184.

5.3. OA 184 as a depolarizing object

There are two bright patches in polarized intensity at 4.8 GHz. One is well inside OA 184 and the other just outside. The polarization angle on each patch is relatively constant and the difference in angle between both patches is between 15 and 20°. Let us assume for the moment that these patches belong to the same structure, the synchrotron filament, and are intrinsically connected. The gap between them is created through depolarization by the H II region. Since the H II region seems to be ring like or shell like the effect is stronger looking tangential to the shell than looking perpendicularly through it. This means that where we see the shell of the H II region the path length through it is longer than in the interior (the geometry in Fig. 8) and so where we see the shell it completely depolarizes the background polarization and in the interior it only rotates the polarization angle. The rotation between the outer patch and the inner one is between 15 and 20 degrees implying an RM between −67 and −89 rad m^{-2}. To completely depolarize the emission we require a rotation of more than 45 degrees in either sense, for which the

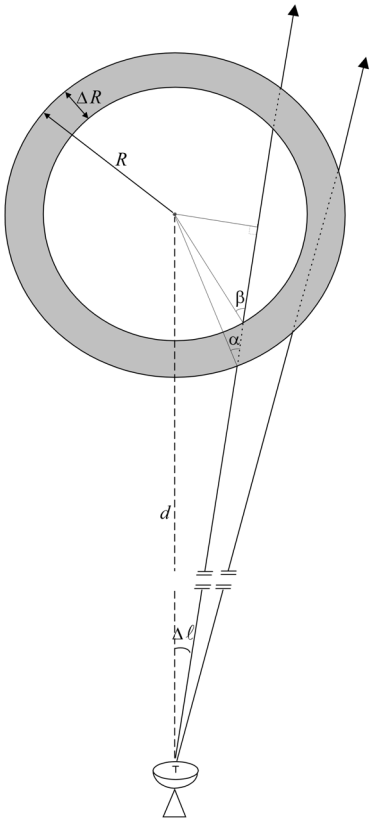

Fig. 8. The viewing geometry used to derive Eq. (3), which describes OA 184 as an ionized shell of finite thickness (ΔR). The viewing angle is $\Delta\ell$ offset from the shell centre, the distance d, and the angles α, β are defined as $\sin\alpha \approx d/R\ \Delta\ell$ and $\sin\beta \approx d/(R-\Delta R)\ \Delta\ell$.

RM must be 2.25 to 3 times higher than in the interior. If we attribute this RM difference to the different path length through the H II region shell only, we would require a shell thickness of less than 0.2 degrees. This agrees with the appearance of OA 184 very nicely.

6. Modelling the thermal emission properties of OA 184

RRL emission from hydrogen near the value predicted by the line-to-continuum ratio ($T_{\rm line}$ = 2 mK) is unquestionably detected from the brightest continuum filament of OA 184 (see Fig. 3). This indicates the radio emission in the shell is entirely thermal in nature. The velocity of OA 184 has been estimated at $v_{\rm LSR} = -30$ km s^{-1} by association with ISM features (Routledge et al. 1986). The central velocity of the recombination line detected towards the shell is -25.8 ± 0.6 km s^{-1}, close to the Hα line published for the object ($v_{\rm LSR} = -30.1$ km s^{-1} Fich et al. 1990), and supportive of the estimate from association with the filamentary neutral hydrogen in this area (-26.8 km s^{-1}, see Fig. 4). The 34.7 ± 4.6 km s^{-1} width of this line well matches the Hα linewidth Δv = 37.5 km s^{-1} (an intrinsic linewidth determined from the value in Fich et al. 1990). This line is perhaps somewhat broader than are typical Galactic H II region lines (25 km s^{-1} is found by Lockman 1989). However, it is unlikely to be due to blending with ISM ionized hydrogen in the beam, as the observed line intensity is that predicted from the background-subtracted continuum temperature of OA 184. The line may also be partially collisionally broadened. This so-called pressure-broadening effect depends on the density $n_{\rm e}$ of the gas in the telescope's beam. Under the prevailing value of $n_{\rm e}$ = 5.4 cm^{-3} (see below), we conclude that pressure broadening will be negligible.

To estimate physical conditions of OA 184, we start by assuming recombination is in local thermodynamic equilibrium (LTE) with ionization, and that the H II is optically thin ($\tau_{\rm line} \ll 1$). Then, the following system of equations (cf. Osterbrock 1974, Eqs. (4.32) and (5.14)) determines the LTE temperature $T_{\rm e}$ and emission measure $EM = \int n_{\rm e}^2 {\rm d}l$ of the gas:

$$T_{\rm line} = 1.01\times10^7 \frac{c\Delta n f_{n,m}}{n\nu_0 \Delta v_{\rm line} T_{\rm e}^{1.5}} EM \quad (1)$$

$$T_{\rm c} = 8.24\times10^{-2} T_{\rm e}^{-0.35} \nu_0^{-2.1} EM \quad (2)$$

where oscillator strengths $f_{n,m}$ for α-transitions (Δn = 1) are tabulated by Goldwire (1968). For ν_0 = 5.6 GHz (H105α), we find $T_{\rm e}$ = 10 200 K, EM = 685 cm^6 pc^{-1}. To estimate the path length dl, the H II region is modelled as a thick shell in Fig. 8 with angular diameter on the sky $2\theta = 1.28°$ (shown in Fig. 2). Then, the path length anywhere on the shell is:

$${\rm d}l = \begin{cases} 2R\left(\sqrt{1-\left(\frac{d}{R}\Delta\ell\right)^2} - \left(1-\frac{\Delta R}{R}\right)\sqrt{1-\left(\frac{d}{(R-\Delta R)}\Delta\ell\right)^2}\right), \\ \qquad \Delta\ell < \theta_{\rm inner} \\ 2R\sqrt{1-\left(\frac{d}{R}\Delta\ell\right)^2},\ \theta_{\rm inner} \le \Delta\ell \le \theta \end{cases} \quad (3)$$

where $\theta_{\rm inner} = 0.53°$ is the angular radius of the inner shell on the sky. The path can be either through the two halves of the shell ($\Delta\ell < \theta_{\rm inner}$) or through the shell wall ($\theta_{\rm inner} \le \Delta\ell \le \theta$, shown in Fig. 8). For the viewing angle of the RRL observations ($\Delta\ell$ = 0.555°), d$l \simeq R$. Assuming a uniform electron distribution in the path through the wall (filling fraction unity), the LTE emission measure derives from $n_{\rm e} \sim 5.5$ cm^{-3}.

What effect will departure from LTE have on our solutions? To estimate this, we multiply Eq. (1) by $b_n\,(1 - kT/h\nu\ {\rm d}\ln b_n/{\rm d}n\ \Delta n)$ (Eq. (5.16) in Osterbrock 1974), and estimate the departure coefficients b_n and d$\ln b_n$/dn from the tables of Salem & Brocklehurst (1979) with the LTE conditions ($\log T_{\rm e} \simeq 4$, $\log n_{\rm e} \simeq 1$) as starting points. We then re-calculate $T_{\rm e}$, $n_{\rm e}$, find the new coefficients, and re-calculate until the solution converges. Numerical convergence is achieved for $T_{\rm e}$ = 8300 K, $n_{\rm e}$ = 5.1 cm^{-3}.

The rotation of the background polarized emission indicates that OA 184 has an ordered component to its magnetic field (within the ionized shell). The shell thickness of 0.11° (Fig. 2) translates to a physical thickness of 3.8 pc (the path length through the shell's face is thus 7.6 pc). In conjunction with the RRL results, we can estimate the electron-weighted mean magnetic field parallel to the line of sight $B_\parallel$ from the rotation measure (RM) through the shell's face:

$$\langle B_\parallel \rangle = \frac{\int n_{\rm e} B_\parallel {\rm d}l}{\int n_{\rm e} {\rm d}l} = \frac{\rm RM}{0.81 {\rm DM}}. \quad (4)$$

The electron density given by the recombination line implies a magnetic field $\langle B_\parallel \rangle = -2$ to 2.5 μG (directed away from the Sun). This is to be regarded as a lower limit to the true field since the RM samples only the component parallel to the line of sight. Nonetheless, our value for $\langle B_\parallel \rangle$ is not inconsistent with other H II regions which have magnetic fields that are weakened due to expansion from their original cool cloud (Heiles et al. 1981).

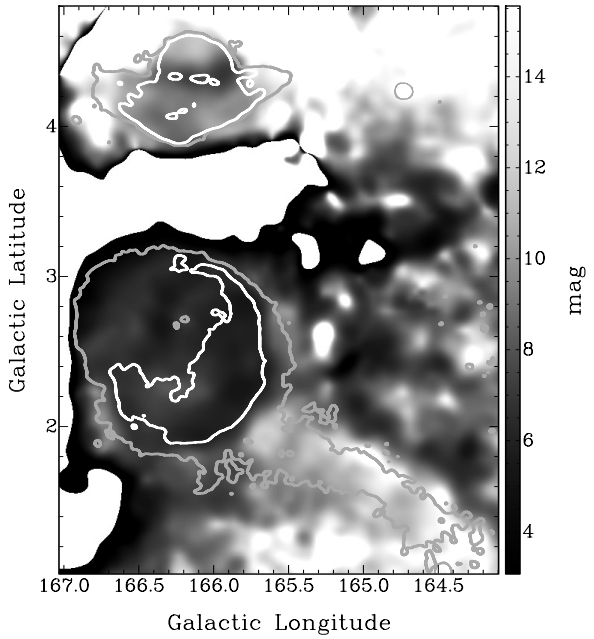

Fig. 9. A map of the optical extinction A_V towards OA 184 and VRO 42.05.01, derived from the ratio of radio-to-optical emission. The 5–6 mag of extinction estimated in this way to OA 184 are much more consistent with estimates of A_V made from the column density of hydrogen nuclei than the 10–12 mag to VRO 42.05.01. Blank areas are where too much background was subtracted and the argument of the logarithm (Eq. (6)) was <0.

7. Extinction and probable exciting star for OA 184

A 6′ resolution map of the region in optical Hα emission has been obtained from the composite map of Finkbeiner (2003). The map of the region contains data from the VTSS (Dennison et al. 1998), and WHAM survey (Haffner et al. 2003), and has been photometrically calibrated, with an uncertainty of ∼0.3 Rayleighs. After removing point sources, the 21 cm CGPS radio map is convolved to 6′, and a surface is fitted to the background and removed from each map. The radio emission measure of the objects EM(21 cm) (calculated with Eq. (2)) is then compared to the optical EM(Hα), given by:

$$\frac{EM(\mathrm{H}\alpha)}{(\mathrm{cm}^6\ \mathrm{pc}^{-1})} = 2.75\left(\frac{T_\mathrm{e}}{(10^4\mathrm{K})}\right)^{0.9}\frac{I_{\mathrm{H}\alpha}}{(\mathrm{Rayleighs})}. \quad (5)$$

The total optical extinction suffered by the emission is then given by the ratio of Eqs. (2) to (5) (e.g. Dickel et al. 1969):

$$A_\mathrm{V} = 1.28 \times 2.512 \log_{10}\left(\frac{EM(21\ \mathrm{cm})}{EM(\mathrm{H}\alpha)}\right). \quad (6)$$

In this way an extinction map of the region is derived (Fig. 9). The map is an upper-limit, as it assumes that all radio emission is thermal in origin. If the radio emission is not entirely thermal, then a fraction of the continuum temperature T_c will not be from free-free emission and not be in the same proportion to the Hα emission as the thermal component. The ratio in Eq. (6) will then give excessive values for A_V.

To determine what is reasonable to expect for A_V here, we use CGPS H I data to measure the column density towards three absorbed continuum sources near OA 184, and convert these to extinction using the dust-to-gas ratio of Vuong et al. (2003) ($1.57 \pm 0.1 \times 10^{21}$ cm^{-2} mag^{-1}). From these, the integrated extinction to the velocity of OA 184 ($v_\mathrm{LSR} = -26$ km s^{-1}) is $A_V = 3$ to 4 mag, and to the Galactic edge 3.5 to 4.8 mag. These estimates of A_V are to be considered as *lower limits*, as we neglect the contribution to the column from molecular hydrogen (^{12}CO CGPS data for this region were not available at the time of this writing).

As has been discussed, a non-thermal filament of emission invades OA 184's boundary, and this is not easily separated from the total 21 cm continuum map. The extinction map of Fig. 9 is an *upper limit* to the true value. Nonetheless, these upper-limits (A_V = 5–6 mag, found across the face of OA 184 in the extinction map of Fig. 9) are *much more* compatible with the lower limits of 3–4 mag (from the H I column), whereas upper limits across VRO 42.05.01 (10–12 mag) *exceed* even the Galactic-edge H I values by 20 dB or more. The difference cannot easily be explained by the absence of the molecular contribution in the column density, nor as due to different extinction to each object (both objects are optically visible; VRO 42.05.01 corresponds to Sh2-224). Clearly, extinction values to OA 184 are more consistent with the integrated hydrogen column density if the radio emission descends from the free-free mechanism.

A Galactic H II region as close as OA 184 should have at least one exciting star visible. An early type star (BD+41°1144) is observed towards the center of the radio shell of OA 184 (see Fig. 5). This star is observed to have spectral type and luminosity class O7.5V by Crampton & Fisher (1974), but not enough photometric colours are available to assess this star's reddening and distance. However, the radial velocity of the star is -26.3 ± 7.4 km s^{-1} (Crampton & Fisher 1974), and while this velocity is cited as possibly variable, it is an exceptional match to the recombination line velocity. If we use the H I column extinction (A_V = 3–4 mag) as surrogate for the extinction of this star, then the distance is 2–3 kpc. Although there are other stars of comparable magnitude in the boundary of OA 184, none are as centrally located as BD+41°1144. If the electron density determined in Sect. 6 is valid throughout the radio shell of OA 184, then the excitation parameter of OA 184 is $U \simeq R \times n_\mathrm{e}^{2/3} \simeq 70$ pc cm^{-2}, approximately that of a single O7.5V star (Churchwell & Walmsley 1973). The centralized location and similar excitation parameter lead us to conclude that the star BD+41°1144 alone is the source of ionizing radiation for OA 184.

8. Summary

The verdict of this paper is that OA 184 is wholly an H II region. This conclusion has been arrived at by augmenting the collection of literature with carefully treated existing data (particularly the radio spectrum), and new observations, all of which tell the tale of thermal emission. To recount our evidence, we find:

- H103-110α RRL emission from the shell of OA 184 at the level predicted by assuming this shell is thermal.
- No observed X-ray emission from OA 184, but significant X-ray emission from nearby SNRs HB 9 and VRO 42.05.01.
- No polarization from the shell at 21 cm and 6 cm (whereas HB 9 and VRO 42.05.01 both show significant polarization at 21 cm).
- No detectable low-frequency radio continuum emission from OA 184 (both HB 9 and VRO 42.05.01 very bright at low frequencies).
- A distinct dust shell at 60 and 100 μm IRAS bands; no detected IR emission from either HB 9 or VRO 42.05.01.

- A flatter radio spectrum (index $\alpha = -0.2$ to -0.14) agreeing more with a thermal emission mechanism than non-thermal.
- An upper-limit optical extinction to OA 184 (predicted by assuming the object is an H II region) that is consistent with the lower limit assessed from H I absorption column densities.
- A single O7.5V star centred within the shell of OA 184, with a similar excitation parameter as the nebula.

The serendipitous arrangement of OA 184 against a polarized Galactic background has shown that an ordered magnetic field runs through the shell of OA 184. The 5 GHz Q and U and RRL data have been used together to estimate this magnetic field, an important measurement that attests to the necessity of high-frequency line and continuum observations for magnetic field studies of the ISM.

Broadly, this study has consequences for our knowledge of the interstellar environment, since one of the largest known SNRs in the Galaxy, and a source once thought of as a significant energy input into the immediate ISM, is gone. Between $\ell = 160°$ and $\ell = 180°$ only four known SNRs remain (HB 9, VRO 42.05.01, G179.0+2.6 and Simeiz 147); the loss of OA 184 as a SNR reduces the presumed energy input here by some ∼20%. Studies such as this one, conducted on other putative supernova remnants, will undoubtedly reveal more misclassified SNRs, and have an impact on the application of current models of SNR-driven ISM astrophysics.

Acknowledgements. We acknowledge our indebtedness to the referee Dr. John Dickel (the co-discoverer of OA 184), who carefully remarked on our manuscript and gave very constructive suggestions. T.F. thanks Dana Balser and Toney Minter of NRAO, Green Bank, for their problem solving skills during the GBT observations, and also acknowledges the efforts of Carl Bignell (NRAO, Green Bank) on our behalf, without which the recombination line results would not have been so outstanding. We thank Tom Landecker (National Research Council Canada) for his careful review of our manuscript. The 6 cm data were obtained with the receiver system from MPIfR mounted at the Nanshan 25-m telescope at the Urumqi Observatory of NAOC. We thank the staff of the Urumqi Observatory of NAOC for the great assistance during observations. We have made use of the ROSAT Data Archive of the Max-Planck-Institut fuer extraterrestrische Physik (MPE) at Garching, Germany. The Dominion Radio Astrophysical Observatory is operated as a national facility by the National Research Council of Canada. The Canadian Galactic Plane Survey is a Canadian project with international partners, and is supported by a grant from the Natural Sciences and Engineering Research Council of Canada (NSERC).

References

Binette, L., Dopita, M. A., Dodorico, S., & Benvenuti, P. 1982, A&A, 115, 315
Burton, W. B., & Hartmann, D. 1994, Ap&SS, 217, 189
Crampton, D., & Fisher, W. A. 1974, Publ. Dominion Astrophys. Obs., 14, 283
Churchwell, E., & Walmsley, C. M. 1973, A&A, 23, 117
Dennison, B., Simonetti, J. H., & Topasna, G. 1998, Publ. Astron. Soc. Austr., 15, 147
Dickel, J. R., & Yang, K. S. 1965, ApJ, 142, 1642
Dickel, H. R., Wendker, H., & Bieritz, J. H. 1969, A&A, 1, 270
Downes, D., & Wilson, T. L. 1974, A&A, 34, 133
Eisenhauer, F., Schödel, R., Genzel, R., et al. 2003, ApJ, 597, L121
Emerson, P. T., & Gräve, R. 1988, A&A, 190, 353
Fesen, R. A., Blair, W. P., & Kirshner, R. P. 1985, ApJ, 292, 29
Fich, M., Treffers, R. R., & Dahl, G. P. 1990, AJ, 99, 622
Finkbeiner, D. P. 2003, ApJS, 146, 407
Foster, T., & MacWilliams, J. 2006, ApJ, 644(1), 214
Fürst, E., Reich, W., Reich, P., & Reif, K. 1990, A&AS, 85, 691
Goldwire, H. C. 1968, ApJS, 17, 445
Green, D. A. 2004, Bull. Astron. Soc. India, 32, 335
Haffner, L. M., Reynolds, R. J., Tufte, S. L., et al. 2003, ApJS, 149, 405
Hartmann, D., & Burton, W. B. 1997, Atlas of Galactic Neutral Hydrogen (Cambridge: Cambridge Univ. Press)
Haslam, C. G. T., & Salter, C. J. 1971, MNRAS, 151, 385
Heiles, C., Chu, Y.-H., & Troland, T. H. 1981, ApJ, 247, L77
Koo, B.-C., & Heiles, C. 1991, ApJ, 382, 204
Kothes, R., Fedotov, K., Foster, T., & Uyaniker, B. 2006, A&A, submitted
Landecker, T. L., Dewdney, P. E., Burgess, T. A., et al. 2000, A&AS, 145, 509
Leahy, D., & Marshall, C. R. 1988, MNRAS, 235, 805
Leahy, D., & Tian, W. 2005, 440, 929
Lockman, F. J. 1989, ApJS, 71, 469
Osterbrock, D. E. 1974, Astrophysics of Gaseous Nebulae (San Francisco: W.H. Freeman & Company)
Padmanabhan, T. 2001, Theoretical Astrophysics (Cambridge University Press), 2, 21
Rohlfs, K. 1986, Tools of Radio Astronomy (Berlin: Spirnger-Verlag), 255
Routledge, D., Landecker, T. L., & Vaneldik, J. F. 1986, MNRAS, 221, 809
Salem, M., & Brocklehurst, M. 1979, ApJS, 39, 633
Sharpless, S. 1959, ApJS, 4, 257
Sun, X. H., Reich, W., Han, J. L., Reich, P., & Wielebinski, R. 2006, A&A, 447(3), 937
Taylor, A. R., Gibson, S. J., Peracaula, M., et al. 2003, AJ, 125, 3145
Vessey, S. J., & Green, D. A. 1998, MNRAS, 294, 607
Vuong, M. H., Montmerle, T., Grosso, N., et al. 2003, A&A, 408, 581
Williams, P. J. S., Kenderdine, S., & Baldwin, J. E. 1966, MNRAS, 70, 53
Woltjer, L. 1972, ARA&A, 10, 129
Xu, Y., Reid, M. J., Zheng, X. W., & Menten, K. M. 2006, Science, 311(5757), 54